Thermal Transistor Effect in Quantum Systems

Antonio Mandarino,[1,2,*] Karl Joulain,[3] Melisa Domínguez Gómez,[3,4] and Bruno Bellomo[1]

[1] *Institut UTINAM, CNRS UMR 6213, Université Bourgogne Franche-Comté, Observatoire des Sciences de l'Univers THETA, 41 bis avenue de l'Observatoire, 25010 Besançon, France*

[2] *International Centre for Theory of Quantum Technologies, University of Gdańsk, 80-308 Gdańsk, Poland*

[3] *Insitut Pprime, CNRS, Université de Poitiers, ISAE-ENSMA, 86962 Futuroscope Chasseneuil, France*

[4] *Instituto de Fisica, Universidad de Antioquia, Calle 70 No. 52-21, Medellin, Colombia*

(Received 13 July 2021; accepted 16 August 2021; published 14 September 2021)

We study a quantum system composed of three interacting qubits, each coupled to a different thermal reservoir. We show how to engineer it to build a quantum device analogous to an electronic bipolar transistor. We outline how the interaction among the qubits plays a crucial role for the appearance of the effect, also linking it to the characteristics of system-bath interactions that govern the decoherence and dissipation mechanisms of the system. By comparison with previous proposals, our model extends the regime of parameters where the transistor effect occurs, the effect being more robust with respect to small variations of the coupling parameters. Moreover, our model appears to be more realistic and directly connected in terms of potential implementations to feasible setups in the domain of quantum spin chains, such as molecular nanomagnets.

DOI: 10.1103/PhysRevApplied.16.034026

I. INTRODUCTION

The exploitation of classical thermodynamics has contributed to the technological revolution that shaped our world since the 19th century [1]. In recent years the exploration of the thermodynamics of quantum systems has given birth to quantum thermodynamics: a high-impact research field both on the fundamental level and on the applicative level [2]. In analogy to classical models, quantum heat engines have been proposed and realized [3–5]. In particular, the properties of nonequilibrium open quantum systems have been used to study how to obtain many-body entanglement [6] or efficient flux management [7]. Moreover, the implementation of nonequilibrium quantum heat machines has been discussed in solid-state setups [8] or in more complex scenarios [9].

The ability to manipulate quantum resources is a demanding but fruitful task that has to be pursued to build useful devices for future application. A potential high-impact apparatus will be one aiming at the control of thermal-energy transport in quantum systems and at the amplification of heat fluxes among the different parts constituting a composite system. A promising approach in the aforementioned task is to pursue the flourishing path followed in electronics after the realization of rectifiers and transistors with semiconducting materials [10] that paved the way to build logic gates and to information and computational technology [11].

Typically, the phenomena of thermal and electric currents are empirically well described by Fourier's law and Ohm's law, respectively. The functional dependence on the two respective control variables, temperature and voltage, is of the same type. Recently, evidence of the emergence of Fourier's law has been pointed out also in the quantum realm [12,13].

The proposal for such thermal analogs of the electronic rectifier and transistor is based on the assumption that in a thermal setup the role played by batteries could be played by thermostats. This analogy allowed various proposals of mesoscopic thermal devices such as rectifiers and diodes [14,15], transistors [16], operating either in the near-field regime [17] or in the far-field regime [18] of thermal radiation, and also thermal logic gates [19,20].

Theoretical efforts are bolstered by experimental ingenuity involving a wide range of experimental platforms ranging from carbon and boron nitride nanotube structures [21] and bulk oxide materials [22] to semiconductor quantum dots [23], magnonic systems [24], and phase-changing materials, such as vanadium dioxide (VO_2) [25,26] and ceramic materials, the latter behaving below a critical temperature like high-temperature superconductors and above it as dielectrics [27,28].

At the same time, the quest for atomic-scale devices for quantum computational purposes is increasingly requiring the necessity to control and manipulate single-atom or

*mandarino.ant@gmail.com

few-atom systems. In particular, the isolation and coherent manipulation of single spins, which are one of the best candidates for a nonoptical implementation of a single qubit, is achieved using optical traps and electrical techniques [29]. Recently, several quantum technology devices have been proposed, including isolators based on photonic transitions [30], rectifiers [31,32], transistors in an electromagnetically controlled environment [33,34], and also phonon-thermoelectric transistors [35]. All the aforementioned platforms have been challenged by the expertise required in chemistry to use single molecules as the building blocks of electronic devices. More than a decade ago, miniaturization was shown to be economically disadvantageous and unhandy using standard lithographic techniques [36]. The idea to use single molecules goes back to a seminal paper in 1974 [37], but only recently have experimental achievements with single molecules as active electronic components been obtained [38–40].

Moreover, quantum systems suffer from an unavoidable coupling to their environment, typically modeled as a thermal reservoir of much larger dimensions than those of the system [41,42]. Despite some detrimental phenomena related to decoherence and dissipation, control and engineering of interacting quantum systems coupled with different thermal baths have led to several studies pointing out how to build the smallest thermal refrigerator [43,44] and how to rectify a thermal current at the quantum level [45–47]. Heat rectification via artificial superconducting atoms was experimentally addressed in Ref. [48]. Moreover, recently, the building blocks of a quantum thermal transistor have been discussed considering an integrable spin-chain model [49], in a qubit-qutrit system [50], in a system with three-body interaction [51], and also examining transient effects [52].

In this paper, we analyze the ability to design a quantum thermal transistor using a spin ring that can, in principle, be implemented on a molecular nanomagnet [53]. In comparison with a previous model [49], we consider a more-complex scenario where the collective quantum behavior of a few spins is expected to play a crucial role in the functioning of the device.

This paper is structured as follows. In Sec. II we examine the spin-ring model, outlining the frameworks where the theoretical model finds direct implementability. This section is also devoted to the quantum dissipative process that allows the system to exchange heat fluxes. In Sec. III we discuss how the proposed systems can be adopted to build a quantum thermal transistor and some limits of their applicability. Having in mind a direct experimental implementation, we address the robustness of the transistor effect against unavoidable fluctuations and perturbations in Sec. IV. Section V concludes the paper with some final remarks and prospects. Some details and further considerations can be found in the Appendixes.

II. THE SPIN-RING MODEL

Quantum critical spin chains have long been considered as one of the best substrates to test and implement quantum devices and future quantum computing. Their main characteristic is to exhibit wide versatility [54]. Considering the most-general model for quantum magnetism, described by the Heisenberg Hamiltonian, one can explore a great variety of universality classes by appropriate tuning of the interaction strengths. Moreover, recent modern developments allow one to realize spin chains of a few atoms having net spin $s = 1/2$, opening the way to the exploitation of the physics of some well-known models, such as the Ising, XY, and XXZ models [55–59].

In parallel, molecular nanomagnets [53] are also attracting more interest as a feasible platform for quantum technological purposes [60]. Specifically, molecular nanomagnets, composed of three main units, have been proved to be useful for quantum thermometry [61] and for coherent manipulation of three-qubit states [62].

Spin chains and nanomagnets are theoretically well described by the same effective Hamiltonian upon fixing of the configuration geometry. Here we consider a system of three qubits of frequency ω_p $(p = L, M, R)$ embedded in a magnetic field, and we introduce the vector of the effective spin operators of any qubit $\hat{\mathbf{S}}_p = (\sigma_p^x, \sigma_p^y, \sigma_p^z)^T$ and the 3×3 matrix $\mathbf{\Lambda}_{pq}$ governing the coupling between the pth spin and the qth spin along different polarization axes, where σ_p^i $(i = x, y, z)$ is the ith Pauli matrix of the pth qubit. A realistic description of a triangular spin chain with a qubit at each vertex labeled L, M, and R, as depicted

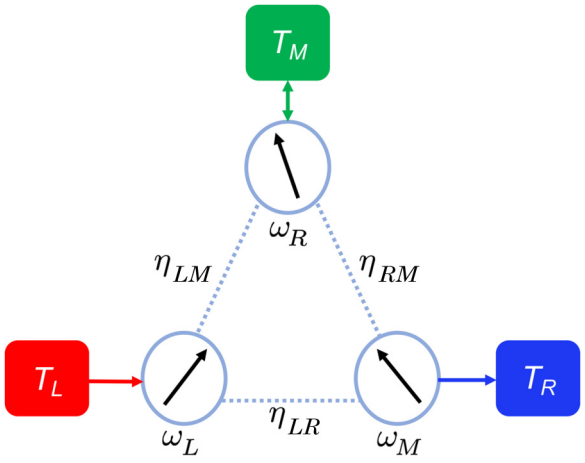

FIG. 1. A system composed by three qubits interacting with each other according to the model in Eq. (2). Each of them is coupled to a different thermal environment as described in Eq. (3).

in Fig. 1, is given by the following Hamiltonian:

$$H_S = \frac{\hbar}{2} \sum_{p=L,M,R} \omega_p \sigma_p^z + \sum_{p \neq q} \hbar \hat{\mathbf{S}}_p^T \mathbf{\Lambda}_{pq} \hat{\mathbf{S}}_q. \quad (1)$$

The first term is the sum of single-particle free Hamiltonians of three qubits immersed in a magnetic field pointing along the direction of the z axis and is responsible of the nonzero field splitting of each qubit. The second term is the intrachain spin-spin exchange coupling. Such a Hamiltonian takes into account symmetric and antisymmetric exchange interactions. A proper tuning of the matrices $\mathbf{\Lambda}_{pq}$ can give a situation where only interactions of the former type occur, as in the standard Heisenberg Hamiltonian, or can introduce a coupling between nonhomologous components of the spin operators, as in the Dzyaloshinskii-Moriya interaction [63,64]. For simplicity, we avoid here the overcomplexity introduced by antisymmetric exchange interaction terms, assuming that the matrices $\mathbf{\Lambda}_{pq}$ are diagonal.

This allows us to consider spins interacting among themselves through a Heisenberg-type Hamiltonian. Therefore, specifying their couplings η_{pq}, with $p, q = L, M, R$ and $p \neq q$, and the strengths along different polarization axes λ^i, we find the Hamiltonian of the system reads

$$H_S = \frac{\hbar}{2} \sum_{p=L,M,R} \omega_p \sigma_p^z + \frac{\hbar}{2} \sum_{p \neq q} \eta_{pq} \sum_{i=x,y,z} \lambda^i \sigma_p^i \sigma_q^i, \quad (2)$$

where η_{pq} and λ^i are part of $\mathbf{\Lambda}_{pq}$, and we have chosen equal λ^i for the three qubits.

A. Comparison between two Ising-type rings

In their seminal paper, Joulain *et al.* [49] addressed how a thermal transistor can be realized with a quantum system of three interacting qubits, each coupled to a thermal reservoir, and showed how it is analogous to an electronic bipolar one. Their discussion is based on a peculiar choice of a very simple model, which implies many strong assumptions on the underlying physics. In that model the magnetic field applied on the three qubits is longitudinal to the direction of the spin-spin interactions. More specifically, this means that in our model the exchange interaction in H_S in Eq. (2) is nonzero only along the same direction of the magnetic field (i.e., only $\lambda^z \neq 0$). Among the other assumptions, this is the one that, in our opinion, requires a detailed discussion. This premise, along with some other minor approximations, has the advantage of allowing the model and the dissipative dynamics to be solvable with analytical techniques, since the operators $\sigma_p^z \sigma_q^z$ commute with the free Hamiltonian. Essentially, the only effect of the zero-field-splitting terms $\sigma_p^z \sigma_q^z$ is to modify the eigenenergies of the system, but the collective eigenfunctions remain the same and can still be expressed as a tensor product of single-particle eigenstates.

It is worth noting that to propose a richer quantum model, a more-complex interaction should be taken into account. The reason why we discuss the class of Hamiltonians defined in Eq. (2), where, in general, the sum of the single-particle contributions does not commute with the interaction term, is twofold: (i) from a purely theoretical point of view, these systems may exhibit strongly correlated and nonlocal eigenstates, opening the door to phenomena with an enhancement due to quantum correlations or quantum fluctuations [54]; (ii) from an experimentally inspired perspective, the control of nanomagnets, spin chains, or even quantum-dot molecules has been well established for quantum critical systems [57–59].

For the aforementioned reasons, our aim is to propose a well-established quantum setting, richer than the one considered in Ref. [49], where the thermal transistor effect is displayed and to study its robustness with respect to the operating temperature and its robustness against spurious fluctuations of the exchange interactions.

In particular, we focus mainly on the case of magnetic systems that belong to the universality class of the quantum critical Ising model in a transverse field and, with abuse of notation, we refer to it as the x-axis Ising model. It can be realized considering in Eq. (2) that the coupling among the qubits acts only along a direction (which we name x) transverse to the applied magnetic field (i.e., only $\lambda^x \neq 0$). This results in a Hamiltonian composed of two terms that cannot be diagonalized in the same basis, in contrast to the model considered in Ref. [49], and such that the collective eigenstates are no longer, in general, factorized states. Once the coupling with the environment is added (see the next subsection), the different directions transverse to the applied magnetic field are not equivalent anymore. Using the same notation as explained above, we refer to the case where only $\lambda^z \neq 0$ as the z-axis Ising model. We address in Sec. IV the presence of perturbations on the x and z configurations.

The x-axis Ising model introduced as the exemplary model to study quantum phase transitions in magnetic systems and their critical behaviors has been used in a wide range of protocols to characterize and fulfill quantum computational tasks [54]. The main feature of such a model resides in the fact that its collective eigenstates are, in general, no longer a tensor product of single-particle states (i.e., they are not separable). Its pivotal role for the comprehension of magnetism at the quantum scale has fostered research into a model magnet where its properties can be experimentally measured with different techniques. The most-germane realization has been achieved in the low-energy magnetic excitation of the insulator $LiHoF_4$ [57] or with crystals of the ferromagnetic $CoNb_2O_6$, where the spin resides on the Co^{2+} ion [58]. A detailed presentation of the spectrum of the x-axis Ising model for the purposes

of this paper is shown in Appendix A, while a complete discussion of the spectrum of the z-axis one can be found in Ref. [49].

B. Dissipative dynamics

Each qubit composing the spin ring described above suffers from an unavoidable coupling with its surrounding environment, which is modeled as a thermal bosonic reservoir. The temperatures T_p of the three reservoirs are, in general, different, giving rise to an out-of-thermal-equilibrium scenario where the temperatures are meant to be tunable at will. The total Hamiltonian is then $H = H_S + H_B + H_I$, where the bath and the system-bath Hamiltonians, respectively, read

$$H_B = \sum_{p=L,M,R} \sum_k \hbar\omega_k a_k^{p\,\dagger} a_k^p,$$
$$H_I = \sum_{p=L,M,R} \sigma_p^x \otimes \sum_k \hbar g_k^p \left(a_k^{p\,\dagger} + a_k^p\right), \tag{3}$$

where a_k^p and $a_k^{p\,\dagger}$ are the bosonic operators of the bath p and g_k^p are the coupling strengths. A schematic representation of the global system is sketched in Fig. 1. As spin-ring Hamiltonian H_S, we consider the one in Eq. (2).

The dynamics of the three-qubit system is dissipative and, under the Born-Markov and secular approximations [41], the evolution of the density matrix is described by a master equation of the following form:

$$\dot{\rho} = -\frac{i}{\hbar}[H_S + H_{\rm LS}, \rho] + \sum_{p=1}^{3} \mathcal{L}_p[\rho], \tag{4}$$

where $H_{\rm LS} = \sum_{p,\omega} \hbar s_p(\omega) A_p^\dagger(\omega) A_p(\omega)$ is the Lamb-shift Hamiltonian, $A_p(\omega) = \sum_{\hbar\omega=\epsilon_i-\epsilon_j} |\epsilon_j\rangle\langle\epsilon_j|\sigma_p^x|\epsilon_i\rangle\langle\epsilon_i|$, $|\epsilon_i\rangle$ with $i = 1, \ldots, 8$ being the dressed states of the Hamiltonian H_S, as described in Appendix A for the case of the x-axis Ising model, and the Lindblad operators are given by [41]

$$\mathcal{L}_p[\rho] = \sum_\omega \gamma(\omega)\left[A_p(\omega)\rho A_p^\dagger(\omega) - \frac{1}{2}\{\rho, A_p^\dagger(\omega)A_p(\omega)\}\right], \tag{5}$$

where $\gamma_p(\omega) = \mathcal{J}_p(\omega)[1 + n_p(\omega)]$ for $\omega > 0$ and $\gamma_p(\omega) = \mathcal{J}_p(|\omega|)n_p(|\omega|)$ for $\omega < 0$. The average number of excitations and the spectral density of the pth reservoir are, respectively, $n_p(\omega) = [\exp(\hbar\omega/k_B T_p) - 1]^{-1}$ and $\mathcal{J}_p(\omega)$, where k_B is the Boltzmann constant. In all the numerical computations, we choose Ohmic reservoirs characterized by a linear spectral density $\mathcal{J}_p(\omega) = \kappa_p\omega$ (at least in the range of working frequencies), using for the three baths independent and possibly different values of κ_p to suitably engineer the effect of the environments on the three qubits. It follows that $\gamma_p(0) = \lim_{\omega\to 0^+} \mathcal{J}_p(\omega)n_p(\omega) = \kappa_p k_B T_p/\hbar$. In Appendix A, a scheme of the transitions induced by the three thermal baths in the case of the x-axis Ising model is also reported.

As we consider a strong coupling between the three qubits (comparable to or greater than the bare frequencies ω_p), we need the above microscopic approach to properly derive the Lindblad operators responsible for the nonunitary evolution of the density matrix, avoiding any extra simplification that can be somehow justified when the spin-spin interactions are much smaller than the bare frequencies of the qubits [41,45,65]. In this limit, we cannot consider phenomenological master equations where the operators $A(\omega)$ are built starting from the eigenstates of the bare system Hamiltonian. For the z-axis Ising model, these coincide with the dressed eigenstates, while for the x-axis Ising model, this is not the case. It has been shown that a phenomenological approach for nonequilibrium systems, ignoring the influence of the intersystem couplings on the dissipators, may lead to scenarios where the second law of thermodynamics may be violated [66].

We also note that since $H_{\rm LS}$ commutes with H_S, it only leads to a renormalization of the unperturbed energy levels of H_S induced by the coupling with the reservoirs and that the steady state is independent of it.

The three temperatures of the environment will, in general, be chosen to be different, leading to out-of-thermal-equilibrium steady states that are not expected to be three-qubit thermal states. At the same time, we expect that each qubit will not thermalize (its own reduced state) to the temperature of its own reservoir because of the collective nature of the quantum dynamics.

In the following sections we perform our analysis using values of the parameters where the derivation of the Markovian secular master equation is well defined.

C. Experimental implementation

The Hamiltonian in Eq. (2) describes the simplest nontrivial example of a spin ring whose properties can be observed with a good approximation in different molecular nanomagnetic systems where any single qubit is represented by one of the three metallic sites as in the $\{Cu_3\}$-type nanomagnet, a complex having almost the shape of an equilateral triangle with a Cu^{2+} ion of spin $-1/2$ at each vertex [67]. Another option is provided by the coupling of individual single-molecule magnets as Cr_7Ni via coordination-chemistry techniques. The ions of these molecular spin clusters, containing one Ni^{2+} ion and seven Cr^{3+} ions, are arranged in a octagonal ring, and their interaction is mediated by fluoride and carboxylate ligands [68]. It has been experimentally proved that such a compound possesses an $s = 1/2$ ground state [69], and it has been

proposed as a suitable candidate to implement a qubit on a molecular substrate [70].

One may wonder about the range of applicability for our purposes of single-molecule magnets. In this case, two major detriments regarding a realistic implementation of our device in molecular systems can be addressed. One concerns the ability to tune the interaction strength among the qubits of the same order of the Zeeman splitting, while the second one concerns how much would be physically accessible to couple locally each qubit to a different thermal bath.

To answer the first question, we refer to the present literature on the engineering of molecular magnetic rings for quantum-technology purposes both theoretically and experimentally. In particular, current experimental techniques, developed within the framework of coordination chemistry, allow one to make the intramolecular and intermolecular couplings tunable [71].

As a suitable candidate, we propose placing the above-described molecular spin cluster Cr_7Ni in any of the three sites of our ring. Its properties as a molecular spin qubit have been deeply investigated in connection with the building up of multiqubit systems via coordination chemistry [68,71], but also its control via electromagnetic fields [72] and the possibility to attach Cr_7Ni rings onto gold surfaces [73]. Whenever possible, one could try to make the Zeeman splitting comparable to the exchange coupling by properly tuning the magnetic field inducing the splitting.

Concerning the second issue regarding a feasible local coupling of any qubit to a different local thermostat, it has never been addressed in the experimental literature on quantum thermal machines. However, many efforts have been devoted to the use of single molecules in electronics as active components to engineer electronic transport. The first coordination complexes elucidating the physics of a single-molecule transistor operated in a regime where single-electron effects, such as Coulomb blockade and Kondo effect, contributed to the assessment of the transistor effect in the quantum regime. The pioneering platform was composed of coordination complexes with a Co ion or a molecule incorporating transition-metal atoms (e.g., the divanadium one). These were subsequently adsorbed on gold surfaces acting as the drain and the source, while the role of the gate potential was played by the tip of an atomic force microscope [74,75]. These studies relying on atomic force microscopy paved the way for the implemention of metal-molecule-metal junctions on other platforms. To mention a few, mechanically controlled and electromigrated break junctions, the design of suitable anchoring groups, and chelating agents such as phthalocyanine have been widely discussed [38–40].

The Hamiltonian in Eq. (2) could be implemented also in other setups, such as in circuit QED [76–78]. In devices of this kid, strong-coupling regimes—namely, ultrastrong and deep-strong ones—are nowadays achieved [79–81] (see also Ref. [82] for an extended review concerning the various coupling regimes of light-matter interaction). As a commentary, we also observe that if the qubits are implemented via an artificial atom, they are typically embedded within a local substrate whose temperature can be manipulated at will. In this case, engineering techniques can be used to make the assumption of local and then independent environments well justified, and characterized in connection to the bath correlation length [83].

III. QUANTUM THERMAL TRANSISTOR

The particular operating principle of an electronic transistor makes it possible to regulate the currents at two of its terminals, which could take very high values, regulating a much-smaller current injected through a third terminal. This peculiarity made the transistor particularly suitable to build logic gates commonly used nowadays in electronics. We propose here a thermal analog of this device able to amplify some of the heat currents circulating in a system as the one in Fig. 1. The control parameter that will play the role of the gate potential in an electronic transistor is the temperature T_M of the reservoir coupled to the middle qubit of frequency ω_M.

A. Heat currents in a thermal transistor

A straightforward way to take into account the heat flow in and out a quantum system [84] is to link the variation of its mean energy $\langle H_S\rangle$ to the sum of the heat currents J_p exchanged between the quantum system and each bath (no power comes from other external sources in our model):

$$\sum_p J_p = \frac{\partial\langle H_S\rangle}{\partial t}. \tag{6}$$

By substituting Eq. (4) into the previous expression, one can compute the current J_p that each thermostat exchanges with the system as

$$J_p = \mathrm{Tr}\left\{\mathcal{L}_p[\rho]H_S\right\}. \tag{7}$$

For the steady state ρ_{SS}, $\dot{\rho}_{SS} = 0$ holds, so $\partial/\partial t\langle H_S\rangle = 0$ and then $\sum_p J_p = 0$. A minor remark concerns the fact that the Lamb-shift term appearing in Eq. (4) does not contribute either to the final expression for J_p or to the steady state, so the steady currents are independent of it. In the following, we always address steady configurations and we use J_p to indicate steady currents.

Following the geometry of the configuration in Fig. 1, we refer to left, middle, and right currents (J_L, J_M, and J_R) as those exchanged, collectively, between the spin ring and, respectively, the left, the middle, and the right thermostat. From now on, we assume that the hot reservoir, providing the energy to the system, is the left one, whereas the cold one, which adsorbs the heat flux, is the one placed

to the right, and the bath in the middle acts as a control. Borrowing the familiar terminology of the bipolar transistor, the left qubit is playing the role of the collector and the right one is playing the role of the emitter, while the middle one is indeed the analog of the base.

B. Conditions to fulfill for a thermal transistor effect

The thermal transistor effect happens when a small change in the control temperature T_M produces a significant variation of the two lateral currents in contrast with a tiny variation of J_M. To study the occurrence of this effect, we define the differential thermal resistances

$$\chi_s = \left(\frac{\partial J_s}{\partial T_M}\right)^{-1}_{T_s=\text{const}}, \quad s = L, R, \tag{8}$$

and, as in the spirit of the electronic transistor [10], we introduce a dynamical amplification factor α_s, a function of the control temperature T_M, defined as

$$\alpha_{L(R)} = \frac{\partial J_{L(R)}}{\partial J_M} = -\frac{\chi_{R(L)}}{\chi_L + \chi_R}. \tag{9}$$

The adimensional parameters in Eq. (9) are the figures of merit used to have a quantitative benchmark for the presence of the thermal transistor effect and they satisfy the relation $\alpha_L + \alpha_R = -1$. In particular, for regions where $|\alpha_s| \gg 1$, one can infer that we are in the presence of a strong amplification of the lateral currents in comparison with the central current. It is easy to see from Eq. (9) that a necessary and sufficient condition to amplify at least one of the two lateral thermal currents is that the two differential thermal resistances, χ_L and χ_R, do not have the same sign. In particular, a strong amplification of both currents is reached if the modulus of χ_L and the modulus of χ_R are almost equal. We underline that conditions of this kind have already been discussed in the context of nonlinear lattices [16], three-terminal graphene devices [85], band-structured engineered silicene superlattices [86], and spin-boson systems [87].

C. Thermal transistor in an *x*-axis Ising model

As said in Sec. II A, the main case we want to discuss is when the three qubits are described by an x-axis Ising model, obtained here by our choosing $\lambda_x = 1$ and $\lambda_y = \lambda_z = 0$. In particular, we firstly choose an open boundary condition where $\eta_{LR} = 0$.

In Fig. 2 we show the behavior of each current as a function of T_M. To deal with adimensional quantities and to take care of a proportionality factor, as explained below, we plot the currents J_p in the unit of $\kappa\hbar\Delta^2$, where $\kappa = \kappa_L$ is the parameter characterizing the strength of the dissipation of the left qubit and $\Delta = \omega_L$, ω_L being assumed to be the reference frequency. The temperature T_M is given

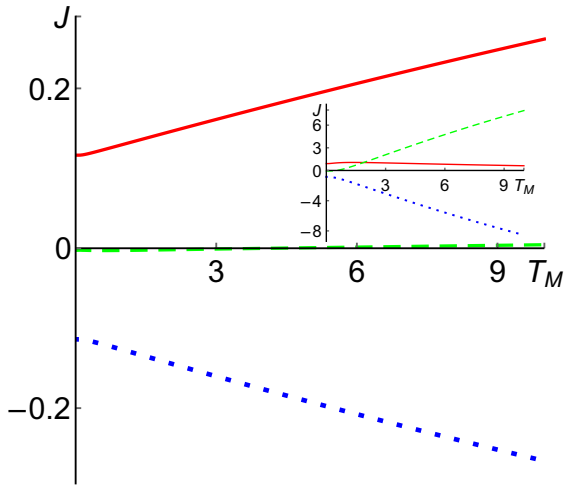

FIG. 2. The three thermal currents defined in Eq. (7) (in the unit of $\kappa\hbar\Delta^2$) exchanged by the environments with the system as a function of the control parameter T_M (in the unit of $\hbar\Delta/k_B$, as for T_L and T_R) when the system is described by an x-axis Ising model ($\lambda_x = 1$ and $\lambda_y = \lambda_z = 0$). The solid red line refers to J_L, the dashed green line to J_M, and the dotted blue line to J_R. The parameters are $\omega_L = \Delta, \omega_M = 0.1\,\Delta, \omega_R = 0.2\,\Delta, \eta_{LM} = \eta_{MR} = \Delta$, $\eta_{LR} = 0$, $\kappa_L = \kappa_M = \kappa, \kappa_R = 100\kappa$, $T_L = 10$, and $T_R = 0.01$. The inset shows the currents in the presence of dephasing as in Eq. (10), with the same color code as in the main plot.

in the unit of $\hbar\Delta/k_B$. Once κ_M and κ_R are also expressed in the unit of κ, the steady state of Eq. (4) is invariant with respect to κ, while the currents are proportional to it. For this reason, we have included κ in the unit used for J_p. Its value must be small enough to guarantee the validity of the approximations used to derive the master equation of Eq. (4). In the following, the values of all currents are always given in the unit of $\kappa\hbar\Delta^2$, while for all the temperatures they are in the unit of $\hbar\Delta/k_B$.

It is possible to appreciate in Fig. 2 how the thermal transistor effect manifests itself and how the amplification of J_L and J_R is continuously achieved.

We stress the crucial role played by the nonequilibrium steady state. The presence of three environments at different temperatures plugged at distant sites in our system is responsible for the three heat flows circulating into it. In particular, it is not surprising to observe that even at $T_M = 0$ each current has a nonzero value. The values used for the couplings are such that we operate in a deep-strong-coupling regime [82]. In the following we use the generic term "strong coupling" to indicate our working region.

To assess the quantum origin of the observed effect, we introduce a suitable modification of the system-bath interaction Hamiltonian in Eq. (3):

$$H_I^{\text{deph}} = \sum_{p=L,M,R} \left(\sigma_p^x + \sigma_p^z\right) \otimes \sum_k \hbar g_k^p \left(a_k^{p\,\dagger} + a_k^p\right), \tag{10}$$

where the added σ_p^z terms account for local dephasing acting on each qubit with the same intensity as the σ_p^x terms. It is clear from the inset in Fig. 2 that in the presence of an extra source of thermal noise inducing dephasing, the thermal transistor effect disappears. This indicates that quantum correlations, destroyed by the added dephasing noise, play a significant role in the functioning of the device observed in the main part of Fig. 2.

To better describe the emergence of the thermal transistor effect observed in the main part of Fig. 2, the amplification factors α_s are plotted in Fig. 3(a), where it is possible to see how the two lateral currents are amplified. Notably, around $T_M \approx 0.600$, the amplification factor diverges, due to a local minimum of J_M, being $J_M \approx -2.90 \times 10^{-3}$. To this extent, we can circumscribe the best working region of the quantum thermal transistor to an interval of the control quantity centered at this value. However, a plateau is present where the amplification factors have values that are still significantly high. In particular, at $T_M \approx 4.17$, where $J_M = 0$ and $J_L = -J_R \approx 0.179$, we have $\alpha_L \approx 18.3$. We notice that for this value of T_M, the reservoir M does not need to inject or absorb energy to maintain the system in the steady state, or in other words, we can say that the central reservoir is in a situation of dynamical thermal equilibrium between the hot and the cold heat baths. This means that all the heat injected by the hot reservoir into the system is transferred directly to the cold bath without any heat-current exchange with the control bath.

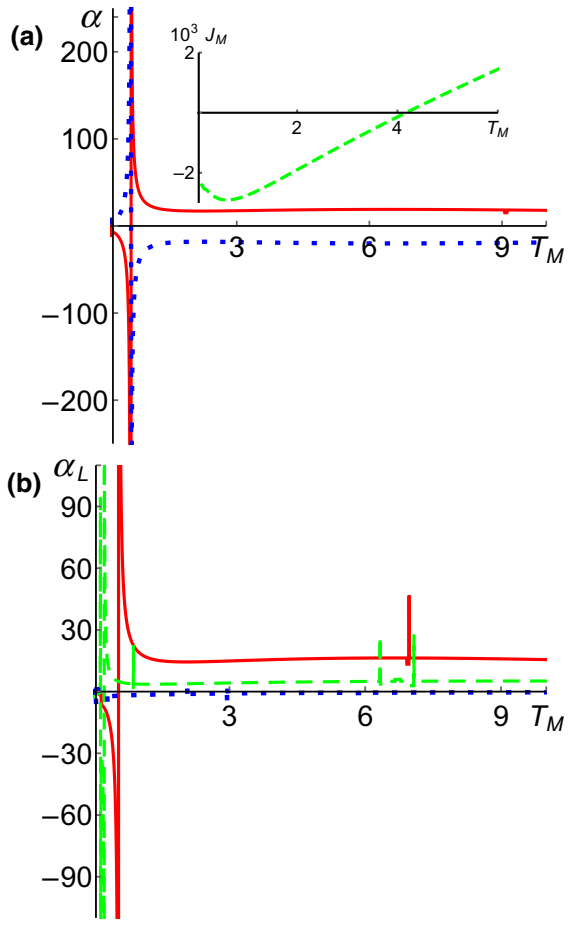

FIG. 3. The amplification factors defined in Eq. (9) as a function of the control parameter T_M (in the unit of $\hbar\Delta/k_B$). In (a), the solid red line refers to α_L and the blue dotted line to α_R. The inset shows J_M (in the unit of $\kappa\hbar\Delta^2$) versus T_M, including the local minimum responsible of the divergence of the amplification factors. The parameters have the same values as in Fig. 2. (b) α_L as a function of T_M for different values of the coupling between the left qubit and the right qubit. The solid red line refers to the case $\eta_{LR} = \Delta/10$, the dashed green line to $\eta_{LR} = \Delta/3$, and the dotted blue line to $\eta_{LR} = \Delta$.

It is easy to see that the right qubit is the one showing $\chi_R < 0$. We have thus shown how a purely quantum scenario can be used to implement a negative-differential-resistance device. Other choices of the values of the parameters entering either in H_S or in the dissipator in Eq. (4) give a behavior of the currents and of the amplifications analogous to the ones in Figs. 2 and 3(a). This is observed in the case of asymmetric configurations.

In Fig. 3(b) we compare different values of the left amplification factor when the interaction between the left qubit and the right qubit is also present (i.e., $\eta_{LR} \neq 0$). In particular, we confirm what was pointed out in Ref. [49], that the thermal transistor effect is still present for different configurations, even if in different zones and with an overall decreased performance when a symmetric configuration is approached (i.e., $\eta_{LM} = \eta_{LR} = \eta_{MR} = \Delta$), for which no amplification of any current is observed. We also notice the appearance of some peaks whose origin could be due to numerical artifacts. Despite our efforts, we cannot exclude this possibility.

We finally stress that the amplification in Fig. 2 is obtained in a regime of strong coupling between the qubits. When the coupling is reduced, smaller currents are found and the performances are spoiled. More details on this analysis are given in Appendix B.

D. Thermal transistor in a z-axis Ising model

To better assess the value of the model proposed here, we compare it with the model studied in Ref. [49], where the thermal transistor effect was observed in a range of temperatures much narrower than in our case. We put ourselves in the same zone of parameters identified in Fig. 2 and we look to see if it is possible to extend the working region to larger zones of temperatures as in the x-axis case.

In Fig. 4 we show that in the case of the z-axis Ising model, obtained here by our choosing $\lambda_x = \lambda_y = 0$ and $\lambda_z = 1$, the thermal transistor effect works only in a narrow interval of the control temperature (namely, $T_M \in [0, 0.35]$), after which the amplification factor drops to values $\alpha_L \lesssim 3.51$. When moving to higher temperatures, we

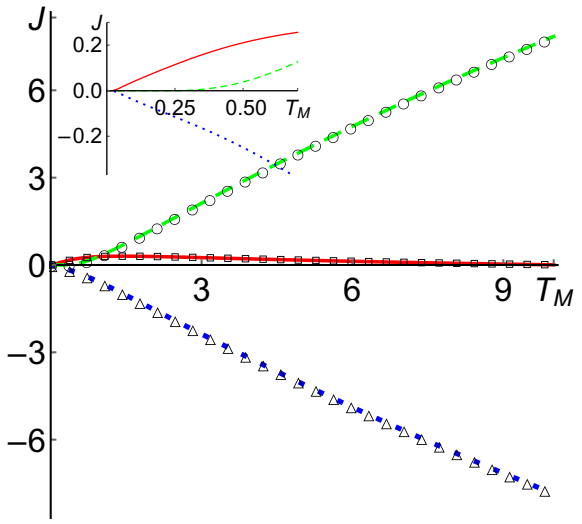

FIG. 4. The three thermal currents defined in Eq. (7) (in the unit of $\kappa\hbar\Delta^2$) exchanged by the environments with the system as a function of the control parameter T_M (in the unit of $\hbar\Delta/k_B$) when the system is described by a z-axis Ising model ($\lambda_x = \lambda_y = 0$ and $\lambda_z = 1$). The solid red line refers to J_L, the dashed green line to J_M, and the dotted blue line to J_R. Empty markers refer to the currents observed in the presence of dephasing as in Eq. (10). Circles, squares, and triangles refer to J_L, J_M, and J_R, respectively. The parameters have the same values as in Fig. 2. The inset shows an enlargement including the working region of this setting.

have strong numerical evidence that the effect completely vanishes, also for different values of the thermal gradient between the hot heat bath and the cold heat bath. In our analysis we also increase the difference $T_R - T_L$ in comparison with what was shown in Ref. [49] and observe that the current amplification is always achieved in the same narrow working region.

It is worth noting that when moving to a regime in which the interqubit coupling is weak, we do not observe a current amplification. As for the x-axis Ising configuration considered in Appendix B, this is due to a sudden thermalization of the left qubit with its corresponding bath (the one at the highest temperature).

We also observe that when a dephasing noise is also present in the dissipative dynamics, the z-axis Ising model is not affected, as shown in Fig. 4. This behavior, in contrast to what is observed in the x-axis Ising model, where dephasing completely destroys the thermal transistor effect, is related to the observations in Sec. II A. It is well known that coherences between the eigenstates of the free Hamiltonian tend to be destroyed by a local dephasing acting on any qubit. Since in the z-axis model the steady state is already diagonal in the basis of the free Hamiltonian, it is not affected when a source of local dephasing noise is introduced. This differs from the case of the x-axis model, where the steady state in the absence of this noise would exhibit coherences in the same local basis of the dephasing mechanism. Even if the x-axis model is fragile with respect to the detrimental effects imposed by the dephasing, we stress in Sec. IV how its truly quantum behavior leads to practical advantages in a realistic scenario in comparison with the z-axis model.

Recently, the appearance of current amplification was discussed in a model based on a qubit-qutrit system [50]. Also in this case, the thermal transistor works in a narrow interval of the control temperature in comparison with the x-axis Ising model analyzed in Sec. III C.

E. Local behavior and local model

Here we discuss the possibility to interpret the results in Fig. 2 on the basis of considerations involving only the local behavior of the qubits composing the spin ring. Firstly, we can have access to some local features introducing the reduced density matrix of any qubit, $\rho_p = \mathrm{Tr}_{q,r\neq p}\{\rho_{\mathrm{SS}}\}$, where ρ_{SS} is the global steady state. We indicate with ρ_p^1 and ρ_p^0, respectively, the populations of the excited state and the ground state of the pth qubit. Each ρ_p is a mixed state in the local energy basis and such that we can define a local temperature for each qubit ($\rho_p^0 \geq \rho_p^1$), with respect to its free Hamiltonian, as

$$T_p^{\mathrm{loc}} = \frac{\hbar\omega_p}{k_B \ln\left(\rho_p^0/\rho_p^1\right)}. \tag{11}$$

We plot in Fig. 5 the local temperatures of the qubits as a function of the control temperature T_M. It is clear that as T_M increases, the temperature gradient between the left and middle qubits decreases, in contrast to what happens between the middle and right quibits. In addition, the external qubits are never in thermal equilibrium with their respective environments, while the middle one reaches equilibrium with the control thermostat M when T_M is equal to T_M^{loc}, which occurs for $T_M \approx 4.37$.

After analysis of the behavior of the local temperatures, we examine if we can qualitatively reproduce the behavior of the global heat currents computed using the model in Sec. II with the following local model. The three qubits are assumed to be in contact with their local thermostats exactly as in our model, but the qubits do not interact between themselves. Instead, each qubit is also coupled, in a stronger way, to another local thermal environment whose temperature is equal to (for any value of T_M) the local temperature $T_p^{\mathrm{loc}}(T_M)$ depicted in Fig. 5. The steady state of each qubit can be made close at will to the thermal state of temperature $T_p^{\mathrm{loc}}(T_M)$ by suitably tuning its coupling with the local thermal reservoir having this temperature. In this local model, the reduced state of each qubit is thus equal to the one obtained in our model, while the way each qubit dissipates heat is greatly different. In the local model the dissipation is governed by local Lindblad

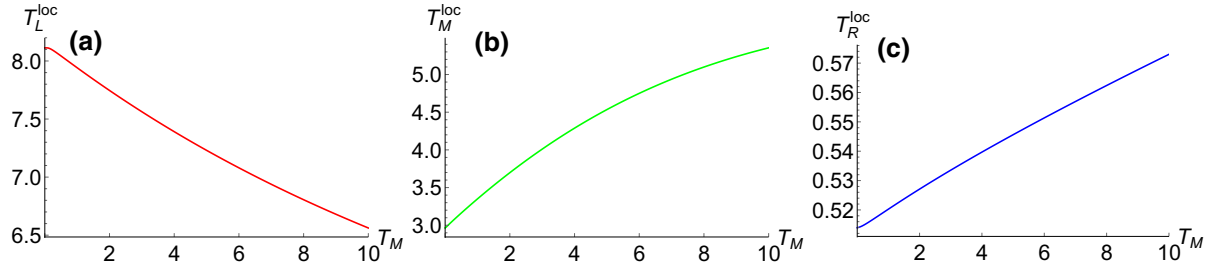

FIG. 5. Local temperatures of the three qubits defined in Eq. (11) as a function of the control parameter T_M (in the unit of $\hbar\Delta/k_B$). The plots in (a)–(c) refer, respectively, to the local temperature of the left qubit, the middle qubit, and the right qubit. The parameters have the same values as in Fig. 2.

operators, while in our model it is governed by collective ones, computed using the dressed states of H_S. We name the currents computed with this local model "local currents".

In Fig. 6 we compare the local currents with the global ones in Fig. 2. We notice that in some cases, local currents well approximate the global ones, such as for J_L, while in other cases they do not, such as for J_R. This is a clear indication of the relevant role played by the collective behavior of the spin ring when it exchanges heat with the local thermostats. The local temperatures induced by the collective dynamics are thus, in general, not enough by themselves to capture all the physics of this collective exchange and of the occurrence of the thermal transistor effect. In particular, we stress the absence of a local minimum for J_M, around which we observed the best performance of the device. We also notice that the middle local current becomes zero for $T_M \approx 4.37$ (i.e., when $T_M = T_M^{loc}$), while the global current J_M becomes zero for $T_M \approx 4.17$.

We also compare the local currents with the global ones when the coupling between the qubits is reduced. We observe that, in general, local currents better approximate the global ones but relevant differences persist. More details are presented in Appendix B.

It is worth noting that this local treatment approach is thermodynamically well justified. Indeed, since in this model the qubits do not interact between themselves, we do not use any kind of local approach, ignoring the interactions among the qubits to take into account the dissipative effects. It is relevant to stress this point since local approaches not taking into account the interactions among the parts of the system can lead to the appearance of nonphysical results as spontaneous flow of the heat from the cold reservoir to the hot reservoir [66].

IV. ROBUSTNESS AGAINST PERTURBATIONS

The results reported in the previous sections show how to build a quantum thermal transistor operating over a wide range of temperatures and starting from a microscopic derivation, with a potential implementation over some feasible physical settings. However, in any real physical implementation of an Ising Hamiltonian, spurious and undesired couplings pointing along different directions of the desired axis for the interaction could occur. This could entail a loss of the thermal transistor effect. Obviously, in any controlled setup, those interactions can be considered as small fluctuations and treated by means of perturbative corrections to the system Hamiltonian H_S. Nevertheless, to pursue our microscopic description of the effect and be precise, we use the full model for the three qubits as in Eq. (2), introducing gradually more-complex interactions and studying to what extent they alter the amplification performances.

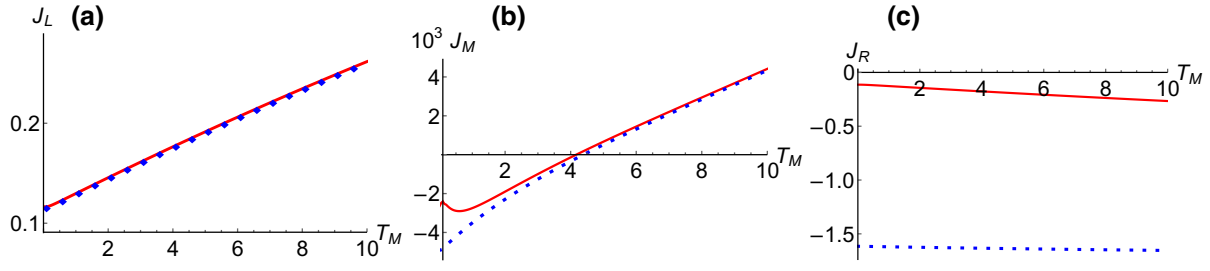

FIG. 6. Comparison between the global currents computed for the x-axis Ising model (red lines), the same ones as in Fig. 2, and the currents obtained with the local model (dotted blue lines) as a function of T_M (in the unit of $\hbar\Delta/k_B$). All the currents are the in unit of $\kappa\hbar\Delta^2$. The plots in (a)–(c) refer, respectively, to the comparison of the current exchanged with the left thermostat, the middle thermostat, and the right thermostat.

To substantiate the process illustrated so far, we consider a physical implementation where the real axis of the interaction term of the model can differ from the expected one (indicated by k in the following) [57], and we compute the amplification factors, $\alpha_s(\lambda^i, \lambda^j)$, which are now functions of the couplings, λ^i and λ^j, along the other two directions i and j, and they may assume a value different from the unperturbed one. Only the coupling between the left and middle qubits and between the right and middle qubits are perturbed, while the coupling between the left and right qubits is maintained equal to zero as before.

To obtain a statistical detailed analysis, we assume that the values of the perturbations are normally distributed and we evaluate the averaged amplification factors

$$\overline{\alpha}_s^{i,j} = \int d\lambda^i d\lambda^j \, \alpha_s\left(\lambda^i, \lambda^j\right) \boldsymbol{\mathcal{N}}\left(\overline{\lambda}^{i,j}, \Sigma^{i,j}\right), \tag{12}$$

where $s = L, R$, and $\boldsymbol{\mathcal{N}}(\overline{\lambda}^{i,j}, \Sigma^{i,j})$ is the bivariate Gaussian distribution of the perturbations. It is centered at their mean values $\overline{\lambda}^{i,j} = (\overline{\lambda}^i, \overline{\lambda}^j)$, with the covariance matrix given by $\Sigma^{i,j} = \mathrm{diag}(\Sigma^i, \Sigma^j)$. In particular, we choose that the spurious interactions can deviate by around 10% from their mean value (i.e., $\Sigma^i = 0.1\overline{\lambda}^i$).

As a tool to investigate the effect of small perturbations, we define the ratio

$$\zeta^{i,j} = \frac{\overline{\alpha}_L^{i,j}}{\alpha_L^{\mathrm{unp}}}, \tag{13}$$

where α_L^{unp} represents the value of the left amplification factor obtained in the absence of perturbation. If only one additional coupling of the type $\sigma_p^i \sigma_q^i$ perturbs the main interaction term $\sigma_p^k \sigma_q^k$, the above ratio is indicated by ζ^i. For clarity, we point out that another quantity analogous to $\zeta^{i,j}$ can, in principle, be defined using the amplification factor of the right current α_R. Nevertheless, its value depends on α_L in a simple way, such that for any T_M this choice would lead to analogues dampings of $\zeta^{i,j}$ as a function of the strength of the perturbation, $\overline{\lambda}^{i,j}$.

In Fig. 7 we show ζ as a function of the average strength of three types of typical perturbations that can occur in both settings discussed in Sec. III. Since α_L^{unp} can diverge for a certain value of the control temperature T_M, we fix it 0.650, close enough to the value where the divergence appears so as to have $\alpha_L^{\mathrm{unp}} \gg 1$ but where it is still finite, being $\alpha_L^{\mathrm{unp}} \approx 1.42 \times 10^3$. We stress that the value of T_M in the presence of perturbations is kept the same as in the unperturbed case. ζ is close to unity when the system still operates as a quantum transistor close to its unperturbed value α_L^{unp} but it vanishes as soon as the perpendicular couplings become more intense.

As is apparent from the plot, the x-axis and z-axis Ising models show completely opposite behavior in the presence of perturbations. Indeed, although both models are perturbed around an optimal configuration, the x-axis model still shows the thermal transistor effect for small-enough extra couplings. In contrast, the possibility to achieve a current amplification with the z-axis Ising model is completely lost in the presence of infinitesimal couplings among the spins in any direction perpendicular to the required interaction axis. Our numerical evidence allows us to see only that ζ is extremely low for values of the extra couplings larger than ten millionths of the one along the z-axis, but we cannot surmise how the unperturbed value is restored for smaller values of the spurious coupling $\overline{\lambda}^{i,j}$.

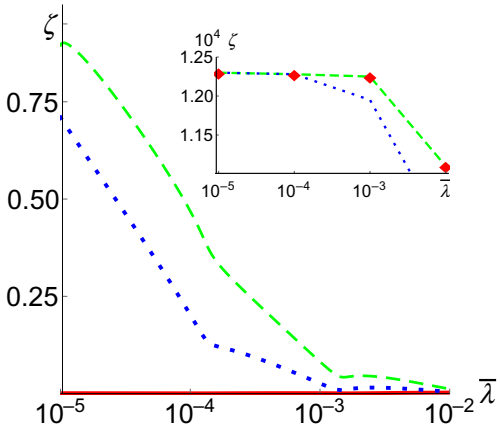

FIG. 7. The ratio ζ defined in Eq. (13) for the x-axis Ising model as a function of the mean value of the spurious couplings $\overline{\lambda}^{i,j}$. The dashed green line refers to ζ^z and the dotted blue line to ζ^y, whereas the red solid line takes into account perturbations with $\bar{\lambda}^y = \bar{\lambda}^z \neq 0$, and then it refers to $\zeta^{y,z}$. The inset shows the ratio ζ for the z-axis Ising model. The dashed green line refers to ζ^x, coinciding with ζ^y (red diamonds). The dotted blue line refers to $\zeta^{x,y}$ and is obtained by our imposing $\bar{\lambda}^y = \bar{\lambda}^z \neq 0$. The parameters of the unperturbed configuration are the same as in Fig. 2. The control temperature T_M is fixed equal to 0.650.

We think that the explanation for the worse resilience of the z-axis Ising model resides mainly in the structure of the couplings between the qubits with respect to their bare Hamiltonian. To give a general commentary, let us write the system Hamiltonian in Eq. (2) as the sum of two terms, $H_S = H_0 + V$, where H_0 is the bare Hamiltonian taking into account the Zeeman splitting of each qubit, and V is the potential that couples the three units composing our system. As pointed out in our discussion of the two possible configurations, a coupling commuting with the bare Hamiltonian, $[H_0, V] = 0$, affects only the eigenfrequencies of the systems, leaving unchanged the eigenstates entering the definition of the operators $A(\omega)$, which are essential to derive the dissipative dynamics of Eq. (4). In the z-axis Ising model, adding to V a perpendicular coupling, not commuting with H_0, completely modifies

the basis in which to expand the operators $A(\omega)$. More specifically, without the perturbation, the eigenstates are factorized in the basis of H_0, while this is not the case when the perturbation is added. It is then reasonable that this specific effect may lead to strong modifications of how noise affects the system. This is not the case for the x-axis Ising model, where already without the perturbation $[H_0, V] \neq 0$ holds, so the dressed basis has already a collective nature. Of course, also in this case it is not equivalent to add a perturbation commuting with H_0 or not commuting with it, because in the latter case we expect stronger differences to appear in the dressed eigenstates. In this sense, it is then easier to justify the results in Fig. 7 showing a better resilience of the x-axis Ising model when a perturbation commuting with H_0 is introduced in contrast to a worse performance when the perturbation is along the y axis.

V. CONCLUSIONS

In this paper, we address the design and the possible physical implementation of a quantum thermal transistor. This device acts on thermal currents as a bipolar electronic transistor does with electric currents, providing an amplification of the collector's and emitter's currents by a proper tuning of the gate potential, while the corresponding gate current is much lower than the other two currents and practically constant.

Our model proposes a system of three qubits strongly interacting among themselves and each of them in contact with a different thermal reservoir. This setting imposes a nonequilibrium dissipative dynamics that entail the presence of nonvanishing steady-state currents flowing into the system via bath-induced transitions. We focus our attention on a particular system that can lead to a feasible realization on several experimental platforms, such as molecular nanomagnets and circuit QED setups, and we refer to this model as the "spin-ring model". In particular, we give some examples of possible single-molecule magnets with different geometry that can serve as a paradigmatic platform and, on the basis of the present literature, we describe how to engineer the required strong coupling and the coupling of nanoscale systems with different thermal reservoirs.

We describe how a quantum thermal transistor works in a scenario where a more-complex spin-spin coupling is present, in comparison with a model recently presented in Ref. [49]. Throughout the paper, we refer to these two models as the "x-axis Ising model" and the "z-axis Ising model". The former is characterized by an interaction Hamiltonian not commuting with the bare one. In particular, the magnetic field acting on the three spins is perpendicular to the direction along which the spins interact. The latter, instead, is a model where the magnetic field and the interactions are longitudinal, so the two contributions of the system Hamiltonian commute.

Choosing as a control parameter the temperature of the heat bath directly coupled to the middle qubit, we show that the x-axis spin ring operates as a thermal transistor over a wider range of temperatures in comparison with the z-axis spin ring. Then we study how the erasure of quantum correlations due to a dephasing noise affects the manifestation of the transistor effect in the two models. The significant amplification of the lateral currents is justified in the context of devices characterized by negative differential thermal resistance [16,85–87] and by means of the collective dynamics. We show that considering a naive local model for the system, which partially takes into account collective phenomena, cannot explain the whole behavior exhibited by our model. Finally, we discuss the robustness of both possible implementations against spurious and uncontrollable couplings stemming from the interaction between different pairs of spins of the spin ring. The results of exact numerical computations suggest that, for reasonably small perturbations, the x-type system can be steered by acting on the control temperature to behave still as a thermal transistor around its unperturbed configuration. In contrast, our computations show that the z-type system is really fragile in the presence of those kinds of perturbations.

As final remark, we stress that our analysis is based on a microscopic derivation of the master equation describing the dissipative dynamics of the system, avoiding any phenomenological simplification. Even if we interpret our findings in terms of the appearance of a negative thermal resistance, we are conscious that a thorough comprehension of the quantum effects contributing to such current amplification is still lacking, due to the plethora of concurring effects that should be present to observe a significant amplification of currents in any realistic scenario. The role of the noncommutativity of the terms in H_S and the role of the dissipation mechanism and how they contribute and compete to give sufficient and necessary conditions for current amplification in dissipative quantum systems could be subjects of future investigations.

ACKNOWLEDGMENTS

A.M. acknowledges the Région Bourgogne-Franche-Comté for financial support throughout Mobility Grant No. 2017Y-06400, the Foundation for Polish Science (FNP) for the IRAP project ICTQT (Contract No. 2018/MAB/5), cofinanced by the EU Smart Growth Operational Programme, and the Polish National Science Center for the grant MINIATURA DEC-2020/04/X/ST2/01794. B.B. acknowledges support by the French Investissements d'Avenir program, project ISITE-BFC (Contract No. ANR-15-IDEX-03). A.M. thanks Heinz-Peter Breuer and Alessandro Lascialfari for useful comments, and Elena Servida for discussions about semiconductor electronics. K.J. and B.B. thank Jose Ordonez-Miranda for useful

discussions. B.B. thanks Benedetto Militello and David Viennot for helpful comments.

APPENDIX A: SPECTRUM OF THE SYSTEM HAMILTONIAN IN THE *x*-AXIS ISING MODEL

Here we give a sketch of the diagonalization of the system Hamiltonian introduced in Eq. (2) and used to obtain the thermal transistor effect discussed throughout the paper. In particular, we focus on the case of the x-axis Ising model with the left and right qubits not interacting (i.e., $\eta_{LR}=0$). We introduce the computational basis, defined as the tensor product $|l_L l_M l_R\rangle$ of all the dispositions of the eigenvectors of the three σ_p^z, satisfying $\sigma_p^z|l_p\rangle = (-1)^{(l_p+1)}\ |l_p\rangle$, with $l_p=0,1$ and $p=L,M,R$. In the basis $\{|111\rangle,|110\rangle,|101\rangle,|100\rangle,|011\rangle,|010\rangle,|001\rangle,|000\rangle\}$, the Hamiltonian H_S of a system composed by three qubits with different splitting in a magnetic field with a transverse Ising interaction (along the x axis) reads

$$\frac{\hbar}{2}\begin{pmatrix}
\Omega_{LM}+\omega_R & 0 & 0 & \Lambda^x_{MR} & 0 & 0 & \Lambda^x_{LM} & 0\\
0 & \Omega_{LM}-\omega_R & \Lambda^x_{MR} & 0 & 0 & 0 & 0 & \Lambda^x_{LM}\\
0 & \Lambda^x_{MR} & \Omega_{LR}-\omega_M & 0 & \Lambda^x_{LM} & 0 & 0 & 0\\
\Lambda^x_{MR} & 0 & 0 & \omega_L-\Omega_{MR} & 0 & \Lambda^x_{LM} & 0 & 0\\
0 & 0 & \Lambda^x_{LM} & 0 & -\omega_L+\Omega_{MR} & 0 & 0 & \Lambda^x_{MR}\\
0 & 0 & 0 & \Lambda^x_{LM} & 0 & \omega_M-\Omega_{LR} & \Lambda^x_{MR} & 0\\
\Lambda^x_{LM} & 0 & 0 & 0 & 0 & \Lambda^x_{MR} & -\Omega_{LM}+\omega_R & 0\\
0 & \Lambda^x_{LM} & 0 & 0 & \Lambda^x_{MR} & 0 & 0 & -\Omega_{LM}-\omega_R
\end{pmatrix}, \tag{A1}$$

where we assume $\eta_{qp}=\eta_{pq}$ and for shorthand we introduce $\Omega_{pq}=\omega_p+\omega_q$ and $\Lambda^x_{pq}=\eta_{pq}\lambda^x$ with $p,q=L,M,R$.

The characteristic equation associated to in Eq. (A1) can be reduced to a quartic equation, leading to four pairs of energy eigenvalues equal in modulus. We can, therefore, decompose H_S in the base where it is diagonal, $H_s=\sum_{i=1}^{8}\epsilon_i|\epsilon_i\rangle\langle\epsilon_i|$, where we order the energy eigenvalues using the following notation: $\epsilon_8\le\epsilon_7\le\cdots\le\epsilon_1$ and $\epsilon_{9-i}=-\epsilon_i$ for all i.

In the computational basis, the eigenvectors of H_S, found for the main case discussed in the paper (see the main part of Fig. 2), are

$$\begin{aligned}
|\epsilon_1\rangle &= -a_1|111\rangle - a_2|100\rangle - a_3|010\rangle - a_4|001\rangle,\\
|\epsilon_8\rangle &= +a_1|000\rangle - a_2|011\rangle + a_3|101\rangle - a_4|110\rangle,\\
|\epsilon_2\rangle &= +b_1|000\rangle + b_2|011\rangle + b_3|101\rangle + b_4|110\rangle,\\
|\epsilon_7\rangle &= +b_1|111\rangle - b_2|100\rangle + b_3|010\rangle - b_4|001\rangle,\\
|\epsilon_3\rangle &= +c_1|000\rangle - c_2|011\rangle - c_3|101\rangle + c_4|110\rangle,\\
|\epsilon_6\rangle &= -c_1|111\rangle - c_2|100\rangle + c_3|010\rangle + c_4|001\rangle,\\
|\epsilon_4\rangle &= +d_1|111\rangle - d_2|100\rangle - d_3|010\rangle + d_4|001\rangle,\\
|\epsilon_5\rangle &= -d_1|000\rangle - d_2|011\rangle + d_3|101\rangle + d_4|110\rangle,
\end{aligned} \tag{A2}$$

where the 16 coefficients a_i,b_i,c_i,d_i with $i=1,2,3,4$ in the above expressions are functions of the parameters entering the Hamiltonian. In all the numerical trials, we find the same structure as above for the eigenvectors, all the coefficients being real.

It is worth noting that the above states have well-defined parity and that the states with opposite energy have different parity. It is easy to check this by measuring the parity operator $P=\sigma_L^z\otimes\sigma_M^z\otimes\sigma_R^z$ on any term appearing in $|\epsilon_i\rangle$.

Finally, we report in Table I the transitions mediated by any thermal reservoir. It is worth noting that we write here only the transitions that can be interpreted as the emission of a photon in the usual context of quantum optics, since they involve states with a positive energy difference between the initial value and the final value.

TABLE I. The possible transitions of positive frequency mediated by any of the three thermal baths by means of the interaction operator σ_p^x for the case in Sec. III C. The first column gives the initial states, starting from the one with highest energy, while the other columns specify the qubit operator coupled to the corresponding thermal reservoir as prescribed by Eq. (3) and the final states connected to the initial ones.

	σ_L^x	σ_M^x	σ_R^x
$\|\epsilon_1\rangle$	$\|\epsilon_2\rangle$, $\|\epsilon_3\rangle$, $\|\epsilon_5\rangle$	$\|\epsilon_2\rangle$, $\|\epsilon_3\rangle$, $\|\epsilon_5\rangle$, $\|\epsilon_8\rangle$	$\|\epsilon_2\rangle$, $\|\epsilon_3\rangle$,$\|\epsilon_5\rangle$
$\|\epsilon_2\rangle$	$\|\epsilon_4\rangle$, $\|\epsilon_6\rangle$	$\|\epsilon_4\rangle$, $\|\epsilon_6\rangle$, $\|\epsilon_7\rangle$	$\|\epsilon_4\rangle$, $\|\epsilon_6\rangle$
$\|\epsilon_3\rangle$	$\|\epsilon_4\rangle$, $\|\epsilon_7\rangle$	$\|\epsilon_4\rangle$, $\|\epsilon_6\rangle$, $\|\epsilon_7\rangle$	$\|\epsilon_4\rangle$, $\|\epsilon_7\rangle$
$\|\epsilon_4\rangle$	$\|\epsilon_8\rangle$	$\|\epsilon_5\rangle$, $\|\epsilon_8\rangle$	$\|\epsilon_8\rangle$
$\|\epsilon_5\rangle$	$\|\epsilon_6\rangle$, $\|\epsilon_7\rangle$	$\|\epsilon_6\rangle$, $\|\epsilon_7\rangle$	$\|\epsilon_6\rangle$, $\|\epsilon_7\rangle$
$\|\epsilon_6\rangle$	$\|\epsilon_8\rangle$	$\|\epsilon_8\rangle$	$\|\epsilon_8\rangle$
$\|\epsilon_7\rangle$	$\|\epsilon_8\rangle$	$\|\epsilon_8\rangle$	$\|\epsilon_8\rangle$

APPENDIX B: WEAK-COUPLING REGIME

Here we address the performances of the system when the interqubit couplings are weak compared with the bare frequencies of the three qubits.

With this aim, we focus in Fig. 8 on the same x-axis-Ising-model configuration ($\lambda_x = 1$ and $\lambda_y = \lambda_z = 0$) discussed in Fig. 2, but we reduce the values of η_{LM} and η_{MR} from Δ to $\eta_{LM} = \eta_{MR} = \Delta/100$. We observe that when the coupling strengths are reduced, the overall performances are spoiled due to the local behavior of the qubit interacting with the hottest reservoir (the left one). Its current vanishes as an effect of the sudden reaching of a thermal equilibrium between the left qubit and its own bath, as is evident in the inset in Fig. 8 where we see that the local temperature of this qubit is always comparable with that of its bath, being $T_L^{\rm loc} \gtrsim 0.9998\ T_L$.

Therefore, we can assess that in the weak-coupling regime the action of the hot bath singles out its homologous qubit from the rest of the system and makes it insensitive to changes of the control parameter. This mechanism is in contrast with the strong-coupling regime, where the collective quantum effects are one of the necessary conditions for the appearance of the thermal transistor effect. We also observe from Fig. 8 that the local model developed in Sec. III E reproduces well the functional behavior of the currents but overestimates (in modulus) the current of the qubit plugged to the cold reservoir. A larger mismatch between the same currents is found in the case of stronger coupling in Fig. 6.

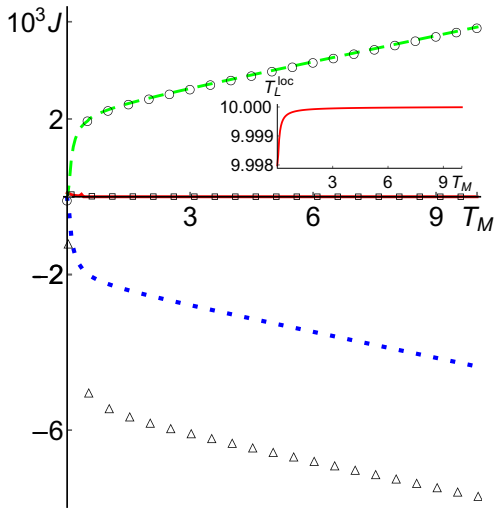

FIG. 8. The three thermal currents defined in Eq. (7) (in the unit of $\kappa\hbar\Delta^2$) exchanged by the environments with the system as a function of the control parameter T_M (in the unit of $\hbar\Delta/k_B$) in the case of the x-axis Ising model ($\lambda_x = 1$ and $\lambda_y = \lambda_z = 0$). The solid red line refers to J_L, the dashed green line to J_M, and the dotted blue line to J_R. The parameters have the same values as in Fig. 2, except for η_{LM} and η_{MR}, whose values are reduced to $\eta_{LM} = \eta_{MR} = \Delta/100$. Empty markers refer to the local currents based on the local temperatures defined in Eq. (11). Circles, squares, and triangles refer to J_L, J_M, and J_R, respectively. The inset shows the local temperature of the left qubit as a function of the control parameter T_M (both in the unit of $\hbar\Delta/k_B$).

[1] S. Carnot, *Réflexions sur la Puissance Motrice du feu et sur les Machines Propres à développer Cette Puissance* (Bachelier, Paris, 1824).

[2] J. Gemmer, M. Michel, and G. Mahler, *Quantum Thermodynamics* (Springer, New York, 2004).

[3] H. T. Quan, Yu-xi Liu, C. P. Sun, and F. Nori, Quantum thermodynamic cycles and quantum heat engines, Phys. Rev. E **76**, 031105 (2007).

[4] R. Uzdin, A. Levy, and R. Kosloff, Equivalence of Quantum Heat Machines, and Quantum-Thermodynamic Signatures, Phys. Rev. X **5**, 031044 (2015).

[5] J. Roßnagel, S. T. Dawkins, K. N. Tolazzi, O. Abah, E. Lutz, F. Schmidt-Kaler, and K. Singer, A single-atom heat engine, Science **352**, 325 (2016).

[6] B. Bellomo and M. Antezza, Nonequilibrium dissipation-driven steady many-body entanglement, Phys. Rev. A **91**, 042124 (2015).

[7] B. Leggio, B. Bellomo, and M. Antezza, Quantum thermal machines with single nonequilibrium environments, Phys. Rev. A **91**, 012117 (2015).

[8] M. Campisi, J. Pekola, and R. Fazio, Nonequilibrium fluctuations in quantum heat engines: Theory, example, and possible solid state experiments, New J. Phys. **17**, 035012 (2015).

[9] R. Alicki and D. Gelbwaser-Klimovsky, Non-equilibrium quantum heat machines, New J. Phys. **17**, 115012 (2015).

[10] J. Bardeen and W. H. Brattain, The transistor, A semiconductor triode, Phys. Rev. **74**, 230 (1948).

[11] J. Millman, *Microelectronics* (McGraw-Hill, New York, 1979).

[12] M. Michel, G. Mahler, and J. Gemmer, Fourier's Law from Schrödinger Dynamics, Phys. Rev. Lett. **95**, 180602 (2005).

[13] D. Manzano, M. Tiersch, A. Asadian, and H. J. Briegel, Quantum transport efficiency and Fourier's law, Phys. Rev. E **86**, 061118 (2012).

[14] M. Terraneo, M. Peyrard, and G. Casati, Controlling the Energy Flow in Nonlinear Lattices: A Model for a Thermal Rectifier, Phys. Rev. Lett. **88**, 094302 (2002).

[15] B. Li, L. Wang, and G. Casati, Thermal Diode: Rectification of Heat Flux, Phys. Rev. Lett. **93**, 184301 (2004).

[16] B. Li, L. Wang, and G. Casati, Negative differential thermal resistance and thermal transistor, Appl. Phys. Lett. **88**, 143501 (2006).

[17] P. Ben-Abdallah and S.-A. Biehs, Near-Field Thermal Transistor, Phys. Rev. Lett. **112**, 044301 (2014).

[18] K. Joulain, Y. Ezzahri, J. Drevillon, and P. Ben-Abdallah, Modulation and amplification of radiative far field heat transfer: Towards a simple radiative thermal transistor, Appl. Phys. Lett. **106**, 133505 (2015).

[19] L. Wang and B. Li, Thermal Logic Gates: Computation with Phonons, Phys. Rev. Lett. **99**, 177208 (2007).

[20] N. Li, J. Ren, L. Wang G. Zhang, P. Hänggi, and B. Li, Colloquium: Phononics: Manipulating heat flow with

electronic analogs and beyond, Rev. Mod. Phys. **84**, 1045 (2012).
[21] C. W. Chang, D. Okawa, A. Majumdar, and A. Zettl, Solid-state thermal rectifier, Science **314**, 1121 (2006).
[22] W. Kobayashi, Y. Teraoka, and I. Terasaki, An oxide thermal rectifier, Appl. Phys. Lett. **95**, 171905 (2009).
[23] R. Scheibner, M. Knig, D. Reuter, A. D. Wieck, C. Gould, H. Buhmann, and L. W. Molenkamp, Quantum dot as thermal rectifier, New J. Phys. **10**, 083016 (2008).
[24] S. Borlenghi, S. Lepri, L. Bergqvist, and A. Delin, Thermo-magnonic diode: Rectification of energy and magnetization currents, Phys. Rev. B **89**, 054428 (2014).
[25] P. J. van Zwol, K. Joulain, P. Ben-Abdallah, and J. Chevrier, Phonon polaritons enhance near-field thermal transfer across the phase transition of VO_2, Phys. Rev. B **84**, 161413(R) (2011).
[26] P. J. van Zwol, L. Ranno, and J. Chevrier, Tuning Near Field Radiative Heat Flux through Surface Excitations with a Metal Insulator Transition, Phys. Rev. Lett. **108**, 234301 (2012).
[27] E. Nefzaoui, K. Joulain, J. Drevillon, and Y. Ezzahri, Radiative thermal rectification using superconducting materials, Appl. Phys. Lett. **104**, 103905 (2014).
[28] J. Ordonez-Miranda, K. Joulain, D. De Sousa Meneses, Y. Ezzahri, and J. Drevillon, Photonic thermal diode based on superconductors, J. Appl. Phys. **122**, 093105 (2017).
[29] R. Hanson and D. D. Awschalom, Coherent manipulation of single spins in semiconductors, Nature (London) **453**, 1043 (2008).
[30] Z. Yu and S. Fan, Complete optical isolation created by indirect interband photonic transition, Nat. Photonics **3**, 91 (2009).
[31] E. Mascarenhas, D. Gerace, D. Valente, S. Montangero, A. Auffèves, and M. F. Santos, A quantum optical valve in a nonlinear-linear resonators junction, Europhys. Lett. **106**, 54003 (2014).
[32] E. Mascarenhas, M. F. Santos, A. Auffèves, and D. Gerace, Quantum rectifier in a one-dimensional photonic channel, Phys. Rev. A **93**, 043821 (2016).
[33] J. Hwang, M. Pototschnig, R. Lettow, G. Zumofen, A. Renn, S. Gtzinger, and V. Sandoghdar, A single-molecule optical transistor, Nature (London) **460**, 76 (2009).
[34] O. V. Astafiev, A. A. Abdumalikov, Jr. A. M. Zagoskin, Yu. A. Pashkin, Y. Nakamura, and J. S. Tsai, Ultimate On-Chip Quantum Amplifier, Phys. Rev. Lett. **104**, 183603 (2010).
[35] J.-H. Jiang, M. Kulkarni, D. Segal, and Y. Imry, Phonon thermoelectric transistors and rectifiers, Phys. Rev. B **92**, 045309 (2015).
[36] R. W. Keyes, Physical limits of silicon transistors and circuits, Rep. Prog. Phys. **68**, 2701 (2005).
[37] A. Aviram and M. A. Ratner, Molecular rectifiers, Chem. Phys. Lett. **29**, 277 (1974).
[38] S. V. Aradhya and L. Venkataraman, Single-molecule junctions beyond electronic transport, Nat. Nanotechnol. **8**, 399 (2013).
[39] L. Sun, Y. A. Diaz-Fernandez, T. A. Geschneidtner, F. Westerlund, S. Lara-Avila, and K. Moth-Poulsen, Single-molecule electronics: from chemical design to functional devices, Chem. Soc. Rev. **43**, 7378 (2014).
[40] H. Song, M. A. Reed, and T. Lee, Single molecule electronic devices, Adv. Mater. **23**, 1583 (2011).
[41] H.-P. Breuer and F. Petruccione, *The Theory of Open Quantum Systems* (Oxford University Press, New York, 2007).
[42] G. Schaller, *Open Quantum Systems Far from Equilibrium* (Springer, Heidelberg, 2014).
[43] N. Linden, S. Popescu, and P. Skrzypczyk, How Small Can Thermal Machines Be? The Smallest Possible Refrigerator, Phys. Rev. Lett. **105**, 130401 (2010).
[44] Z.-X. Man and Y.-J. Xia, Smallest quantum thermal machine: The effect of strong coupling and distributed thermal tasks, Phys. Rev. E **96**, 012122 (2017).
[45] T. Werlang, M. A. Marchiori, M. F. Cornelio, and D. Valente, Optimal rectification in the ultrastrong coupling regime, Phys. Rev. E **89**, 062109 (2014).
[46] T. Chen and X.-B. Wang, Thermal rectification in the nonequilibrium quantum-dots-system, Phys. E (Amsterdam) **72**, 58 (2015).
[47] J. Ordonez-Miranda, Y. Ezzahri, and K. Joulain, Quantum thermal diode based on two interacting spinlike systems under different excitations, Phys. Rev. E **95**, 022128 (2017).
[48] J. Senior, A. Gubaydullin, B. Karimi, J. T. Peltonen, J. Ankerhold, and J. P. Pekola, Heat rectification via a superconducting artificial atom, Commun. Phys. **3**, 40 (2020).
[49] K. Joulain, J. Drevillon, Y. Ezzahri, and J. Ordonez-Miranda, Quantum Thermal Transistor, Phys. Rev. Lett. **116**, 200601 (2016).
[50] B.-Q. Guo, T. Liu, and C.-S. Yu, Quantum thermal transistor based on qubit-qutrit coupling, Phys. Rev. E **98**, 022118 (2018).
[51] B.-Q. Guo, T. Liu, and C.-S. Yu, Multifunctional quantum thermal device utilizing three qubits, Phys. Rev. E **99**, 032112 (2019).
[52] R. Ghosh, A. Ghoshal, and U. Sen, Quantum thermal transistors: Operation characteristics in steady state versus transient regimes, Phys. Rev. A **103**, 052613 (2021).
[53] J. Bartolomè, F. Luis, J. F. Fernández editors, *Molecular Magnets: Physics and Applications* (Springer, 2014).
[54] L. Amico, R. Fazio, A. Osterloh, and V. Vedral, Entanglement in many-body systems, Rev. Mod. Phys. **80**, 517 (2008).
[55] A. A. Khajetoorians, J. Wiebe, B. Chilian, S. Lounis, S. Blügel, and R. Wiesendanger, Atom-by-atom engineering and magnetometry of tailored nanomagnets, Nat. Phys. **8**, 497 (2012).
[56] R. Toskovic, R. van den Berg, A. Spinelli, I. S. Eliens, B. van den Toorn, B. Bryant, J.-S. Caux and, and A. F. Otte, Atomic spin-chain realization of a model for quantum criticality, Nat. Phys. **12**, 656 (2016).
[57] D. Bitko, T. F. Rosenbaum, and G. Aeppli, Quantum Critical Behavior for a Model Magnet, Phys. Rev. Lett. **77**, 940 (1996).
[58] N. Roch, S. Florens, V. Bouchiat, W. Wernsdorfer, and F. Balestro, Quantum phase transition in a single-molecule quantum dot, Nature (London) **453**, 633 (2008).
[59] R. Coldea, D. A. Tennant, E. M. Wheeler, E. Wawrzynska, D. Prabhakaran, M. Telling, K. Habicht, P. Smeibidl, and K. Kiefer, Quantum criticality in an ising chain: Experimental

evidence for emergent E_8 symmetry, Science **327**, 177 (2010).
[60] F. Troiani and P. Zanardi, Size of linear superpositions in molecular nanomagnets, Phys. Rev. B **88**, 094413 (2013).
[61] G. Salvatori, A. Mandarino, and M. G. A. Paris, Quantum metrology in Lipkin-Meshkov-Glick critical systems, Phys. Rev. A **90**, 022111 (2014).
[62] M. D. Jenkins, Y. Duan, B. Diosdado, J. J. García-Ripoll, A. Gaita-Ariño, C. Giménez-Saiz, P. J. Alonso, E. Coronado, and F. Luis, Coherent manipulation of three-qubit states in a molecular single-ion magnet, Phys. Rev. B **95**, 064423 (2017).
[63] I. Dzyaloshinsky, A thermodynamic theory of "weak" ferromagnetism of antiferromagnetics, J. Phys. Chem. Solids **4**, 241 (1958).
[64] T. Moriya, Anisotropic superexchange interaction and weak ferromagnetism, Phys. Rev. **120**, 91 (1960).
[65] G. L. Giorgi, A. Saharyan, S. Guérin, D. Sugny, and B. Bellomo, Microscopic and phenomenological models of driven systems in structured reservoirs, Phys. Rev. A **101**, 012122 (2020).
[66] A. Levy and R. Kosloff, The local approach to quantum transport may violate the second law of thermodynamics, Europhys. Lett. **107**, 20004 (2014).
[67] K.-Y. Choi, Y. H. Matsuda, H. Nojiri, U. Kortz, F. Hussain, A. C. Stowe, C. Ramsey, and N. S. Dalal, Observation of a Half Step Magnetization in the $\{Cu_3\}$-Type Triangular Spin Ring, Phys. Rev. Lett. **96**, 107202 (2006).
[68] G. A. Timco, S. Carretta, F. Troiani, F. Tuna, R. J. Pritchard, C. A. Muryn, E. J. L. McInnes, A. Ghirri, and A. Candini, and P. Santini *et al.*, Engineering the coupling between molecular spin qubits by coordination chemistry, Nat. Nanotech. **4**, 173 (2009).
[69] S. Carretta, P. Santini, G. Amoretti, T. Guidi, J. R. D. Copley, Y. Qiu, R. Caciuffo, G. Timco, and R. E. P. Winpenny, Quantum Oscillations of the Total Spin in a Heterometallic Antiferromagnetic Ring: Evidence from Neutron Spectroscopy, Phys. Rev. Lett. **98**, 167401 (2007).
[70] F. Troiani, M. Affronte, S. Carretta, P. Santini, and G. Amoretti, Proposal for Quantum Gates in Permanently Coupled Antiferromagnetic Spin Rings without Need of Local Fields, Phys. Rev. Lett. **94**, 190501 (2005).
[71] A. Ardavan, A. M. Bowen, A. Fernandez, A. J. Fielding, D. Kaminski, F. Moro, C. A. Muryn, M. D. Wise, A. Ruggi, and E. J. L. McInnes *et al.*, Engineering coherent interactions in molecular nanomagnet dimers, npj Quantum Inf. **1**, 15012 (2015).
[72] J. Liu, J. Mrozek, W. K. Myers, G. A. Timco, R. E. P. Winpenny, B. Kintzel, W. Plass, and A. Ardavan, Electric Field Control of Spins in Molecular Magnets, Phys. Rev. Lett. **122**, 037202 (2019).
[73] V. Corradini, R. Biagi, U. del Pennino, V. De Renzi, A. Gambardella, Marco Affronte, C. A. Muryn, G. A. Timco, and R. E. P. Winpenny, Isolated heterometallic Cr_7Ni rings grafted on Au(111) surface, Inorg. Chem. **46**, 4937 (2007).
[74] J. Park, A. N. Pasupathy, J. I. Goldsmith, C. Chang, Y. Yaish, J. R. Petta, M. Rinkoski, J. P. Sethna, H. D. Abruña, and P. L McEuen *et al.*, Coulomb blockade and the Kondo effect in single-atom transistors, Nature (London) **417**, 722 (2002).
[75] W. Liang, M. P. Shores, M. Bockrath, J. R. Long, and H. Park, Kondo resonance in a single-molecule transistor, Nature (London) **417**, 725 (2002).
[76] O. Viehmann, J. von Delft, and F. Marquardt, Observing the Nonequilibrium Dynamics of the Quantum Transverse-Field Ising Chain in Circuit QED, Phys. Rev. Lett. **110**, 030601 (2013).
[77] Y. Zhang, L. Yu, J.-Q Liang, G. Chen, S. Jia, and F. Nori, Quantum phases in circuit QED with a superconducting qubit array, Sci. Rep. **4**, 4083 (2014).
[78] Y. Salathé, M. Mondal, M. Oppliger, J. Heinsoo, P. Kurpiers, A. Potočnik, A. Mezzacapo, U. Las Heras, L. Lamata, and E. Solano *et al.*, Digital Quantum Simulation of Spin Models with Circuit Quantum Electrodynamics, Phys. Rev. X **5**, 021027 (2015).
[79] T. Niemczyk, F. Deppe, H. Huebl, E. P. Menzel, F. Hocke, M. J. Schwarz, J. J. Garcia-Ripoll, D. Zueco, T. Hümmer, and E. Solano *et al.*, Circuit quantum electrodynamics in the ultrastrong-coupling regime, Nat. Phys. **6**, 772 (2010).
[80] A. Baust, E. Hoffmann, M. Haeberlein, M. J. Schwarz, P. Eder, J. Goetz, F. Wulschner, E. Xie, L. Zhong, and F. Quijandría *et al.*, Ultrastrong coupling in two-resonator circuit QED, Phys. Rev. B **93**, 214501 (2016).
[81] F. Yoshihara, T. Fuse, S. Ashhab, K. Kakuyanagi, S. Saito, and K. Semba, Superconducting qubit–oscillator circuit beyond the ultrastrong-coupling regime, Nat. Phys. **13**, 44 (2017).
[82] P. Forn-Díaz, L. Lamata, E. Rico, J. Kono, and E. Solano, Ultrastrong coupling regimes of light-matter interaction, Rev. Mod. Phys. **91**, 25005 (2019).
[83] F. Galve, A. Mandarino, M. G. A. Paris, C. Benedetti, and R. Zambrini, Microscopic description for the emergence of collective dissipation in extended quantum systems, Sci. Rep. **7**, 42050 (2017).
[84] R. Kosloff, Quantum thermodynamics: A dynamical viewpoint, Entropy **15**, 2100 (2013).
[85] Y. Wu, D. B. Farmer, W. Zhu, S.-J. Han, C. D. Dimitrakopoulos, A. A. Bol, P. Avouris, and Y.-M. Lin, Three-terminal graphene negative differential resistance devices, ACS Nano **6**, 2610 (2012).
[86] C.-H. Chen, W.-W. Li, Y.-M. Chang, C.-Y. Lin, S.-H. Yang, Y. Xu, and Y.-F. Lin, Negative-Differential-Resistance Devices Achieved by Band-Structure Engineering in Silicene under Periodic Potentials, Phys. Rev. Appl. **10**, 044047 (2018).
[87] C. Wang, X.-M. Chen, K.-W. Sun, and J. Ren, Heat amplification and negative differential thermal conductance in a strongly coupled nonequilibrium spin-boson system, Phys. Rev. A **97**, 052112 (2018).